A&A 556, A29 (2013)
DOI: 10.1051/0004-6361/201220846


Astronomy & Astrophysics

# Obscured AGN at $z \sim 1$ from the zCOSMOS-Bright Survey

## I. Selection and optical properties of a [Ne v]-selected sample

M. Mignoli[1], C. Vignali[2], R. Gilli[1], A. Comastri[1], G. Zamorani[1], M. Bolzonella[1], A. Bongiorno[3], F. Lamareille[4,5], P. Nair[1,6], L. Pozzetti[1], S. J. Lilly[7], C. M. Carollo[7], T. Contini[4,5], J.-P. Kneib[8], O. Le Fèvre[8], V. Mainieri[9], A. Renzini[10], M. Scodeggio[11], S. Bardelli[1], K. Caputi[12], O. Cucciati[13], S. de la Torre[14], L. de Ravel[14], P. Franzetti[11], B. Garilli[11], A. Iovino[13], P. Kampczyk[7], C. Knobel[7], K. Kovač[7], J.-F. Le Borgne[4,5], V. Le Brun[8], C. Maier[7,15], R. Pellò[4,5], Y. Peng[6], E. Perez Montero[4,5], V. Presotto[13], J. D. Silverman[16], M. Tanaka[16], L. Tasca[8], L. Tresse[8], D. Vergani[17], E. Zucca[1], R. Bordoloi[7], A. Cappi[1], A. Cimatti[2], A. M. Koekemoer[6], H. J. McCracken[18], M. Moresco[2], and N. Welikala[19]

[1] INAF – Osservatorio Astronomico di Bologna, via Ranzani 1, 40127 Bologna, Italy
e-mail: marco.mignoli@oabo.inaf.it
[2] Dipartimento di Fisica e Astronomia, Università degli Studi di Bologna, viale Berti Pichat 6/2, 40127 Bologna, Italy
[3] INAF – Osservatorio Astronomico di Roma, 00040 Monteporzio Catone, Italy
[4] Institut de Recherche en Astrophysique et Planétologie, CNRS, 31400 Toulouse, France
[5] IRAP, Université de Toulouse, UPS-OMP, Toulouse, France
[6] Space Telescope Science Institute, Baltimore, MD 21218, USA
[7] Institute of Astronomy, ETH Zurich, 8093 Zürich, Switzerland
[8] Laboratoire d'Astrophysique de Marseille, Aix-Marseille Université, CNRS, Marseille, France
[9] European Southern Observatory, Garching, Germany
[10] INAF – Osservatorio Astronomico di Padova, Padova, Italy
[11] INAF – Istituto di Astrofisica Spaziale e Fisica Cosmica, Milano, Italy
[12] Kapteyn Astronomical Institute, University of Groningen, 9700 AV Groningen, The Netherlands
[13] INAF – Osservatorio Astronomico di Brera, Milano, Italy
[14] Institute for Astronomy, The University of Edinburgh, Royal Observatory, Edinburgh, EH93HJ, UK
[15] University of Vienna, Department of Astronomy, 1180 Vienna, Austria
[16] Kavli Institute for the Physics and Mathematics of the Universe, The University of Tokyo, 277-8583 Kashiwa, Japan
[17] INAF – Istituto di Astrofisica Spaziale e Fisica Cosmica, Bologna, Italy
[18] Institut d'Astrophysique de Paris, Université Pierre & Marie Curie, 75014 Paris, France
[19] Institut d'Astrophysique Spatiale, Bâtiment 121, CNRS & Univ. Paris Sud XI, 91405 Orsay Cedex, France

Received 4 December 2012 / Accepted 25 May 2013

**ABSTRACT**

*Aims.* The application of multi-wavelength selection techniques is essential for obtaining a complete and unbiased census of active galactic nuclei (AGN). We present here a method for selecting $z \sim 1$ obscured AGN from optical spectroscopic surveys.
*Methods.* A sample of 94 narrow-line AGN with $0.65 < z < 1.20$ was selected from the 20k-Bright zCOSMOS galaxy sample by detection of the high-ionization [Ne v] $\lambda$3426 line. The presence of this emission line in a galaxy spectrum is indicative of nuclear activity, although the selection is biased toward low absorbing column densities on narrow-line region or galactic scales. A similar sample of unobscured (type 1 AGN) was collected applying the same analysis to zCOSMOS broad-line objects. This paper presents and compares the optical spectral properties of the two AGN samples. Taking advantage of the large amount of data available in the COSMOS field, the properties of the [Ne v]-selected type 2 AGN were investigated, focusing on their host galaxies, X-ray emission, and optical line-flux ratios. Finally, a previously developed diagnostic, based on the X-ray-to-[Ne v] luminosity ratio, was exploited to search for the more heavily obscured AGN.
*Results.* We found that [Ne v]-selected narrow-line AGN have Seyfert 2-like optical spectra, although their emission line ratios are diluted by a star-forming component. The ACS morphologies and stellar component in the optical spectra indicate a preference for our type 2 AGN to be hosted in early-type spirals with stellar masses greater than $10^{9.5-10}\,M_{\odot}$, on average higher than those of the galaxy parent sample. The fraction of galaxies hosting [Ne v]-selected obscured AGN increases with the stellar mass, reaching a maximum of about 3% at $\approx 2 \times 10^{11}\,M_{\odot}$. A comparison with other selection techniques at $z \sim 1$, namely the line-ratio diagnostics and X-ray detections, shows that the detection of the [Ne v] $\lambda$3426 line is an effective method for selecting AGN in the optical band, in particular the most heavily obscured ones, but cannot provide a complete census of type 2 AGN by itself. Finally, the high fraction of [Ne v]-selected type 2 AGN not detected in medium-deep (≈100–200 ks) Chandra observations (67%) is suggestive of the inclusion of Compton-thick (i.e., with $N_{\rm H} > 10^{24}$ cm$^{-2}$) sources in our sample. The presence of a population of heavily obscured AGN is corroborated by the X-ray-to-[Ne v] ratio; we estimated, by means of an X-ray stacking technique and simulations, that the Compton-thick fraction in our sample of type 2 AGN is $43 \pm 4$% (statistical errors only), which agrees well with standard assumptions by XRB synthesis models.

**Key words.** galaxies: active – X-rays: galaxies

## 1. Introduction

The study of the history of accretion is essential for our understanding of how supermassive black holes (SMBHs) form and evolve. Accretion onto an SMBH is the predominant source of energy emitted by active galactic nuclei (AGN), therefore a comprehensive census of AGN of all types across a large portion of cosmic time provides constraints on the current black-hole mass function (Soltan 1982; Rees 1984; Marconi et al. 2004).

Today, there is strong observational evidence that all massive galaxies in the local Universe host a central SMBH (Kormendy & Richstone 1995). This, along with the now firmly established discovery that the masses of SMBHs are proportional to the velocity dispersions and masses of their host stellar spheroids (Magorrian et al. 1998; Ferrarese & Merritt 2000; Gebhardt et al. 2000; Tremaine et al. 2002), indicates an enduring physical connection between nuclear activity and galaxy formation and evolution. Many theoretical and observational efforts have been undertaken recently to comprehend the elusive evolutionary connection between AGN and their host galaxies. Nevertheless, the mechanisms driving this co-evolution are still far from being fully understood. Once again, to clarify the role played by AGN in this symbiosis requires a complete survey of both unobscured and obscured AGN.

Active galactic nuclei present a wide variety of observed properties. They inhabit host galaxies of different morphologies, and show a wide range of luminosities in all wavebands, from radio to X-rays. In the optical/UV range, AGN are characterized by a power-law continuum and broad (>1000 km s$^{-1}$) emission lines, the latter produced in the so-called broad-line region (BLR), extending on scales of light days. These unobscured (type 1) AGN are thus easily identified from their optical spectra. Conversely, there are obscured (type 2) AGN that show only narrow (<1000 km s$^{-1}$) emission lines emerging from the narrow-line region (NLR), with scales on the order of hundreds of light years. Because in these AGN the continuum is often dominated by stellar emission, their optical spectra are similar to those of normal star-forming galaxies (SFGs). According to the standard unified model (Antonucci 1993), this broad classification into two spectral classes depends on whether the central SMBH, its associated continuum, and the BLR are viewed directly (type 1 AGN) or are obscured by a dusty circumnuclear medium (type 2 AGN).

The optical classification of emission-line galaxies is usually made through emission-line ratio diagnostic diagrams. Baldwin et al. (1981) were the first to apply such a technique (BPT), using the strongest emission lines to separate objects into categories according to the excitation mechanism of the emitting gas. In particular, the [O III]/H$\beta$ versus [N II]/H$\alpha$ diagram became the benchmark for emission-line classification, since it can reliably distinguish SFGs, Seyfert 2 galaxies, low-ionization nuclear emission regions (hereafter LINERs, see Heckman 1980), and composite objects with both an AGN and star-forming regions. At redshifts greater than $z \approx 0.5$, the emission lines around H$\alpha$ become redshifted out of the optical window and classical BPT diagrams can no longer be applied. Therefore, diagnostic diagrams need to be based on emission lines observed in the blue part of the galaxy spectrum: [O III], H$\beta$, and [O II] (Rola et al. 1997). Unfortunately, these diagrams are only moderately effective in distinguishing between starbursts and AGN (Stasiñska et al. 2006) and in particular, almost fail to separate LINERS from SFGs (Bongiorno et al. 2010; Lamareille 2010).

The X-ray emission is probably the most prominent characteristic of AGN activity, because X-rays are thought to originate from the innermost regions of an accretion disk around the central SMBH. Combined with observations at different wavelengths, deep wide-field X-ray surveys have been effective indeed in discovering a large proportion of the AGN population, significantly improving our census of AGN demographics (Brandt & Hasinger 2005, and references therein). However, a large population of heavily obscured AGN, predicted by synthesis models for the cosmic X-ray background (XRB; Gilli et al. 2007), is still undetected in X-ray surveys. Although X-ray observations are the least biased against moderately obscured AGN, still even the deepest X-ray surveys can undersample the population of extremely obscured AGN, i.e., those with column densities $N_{\rm H} > 10^{24}$ cm$^{-2}$ (Compton-thick sources).

The emission line [Ne v] $\lambda$3426 can be considered a reliable signature for nuclear activity, given that the ionization potential of Ne4+ is ≈97 eV, and stars generally do not emit photons beyond 55 eV (Haehnelt et al. 2001). Along with the [Ne v] $\lambda$3426 line, the [Ne v] $\lambda$3346 line arises from the same excitation level, but with a relative intensity of approximately one-third (Vanden Berk et al. 2001). A [Ne v]-selected AGN sample should not be affected by significant contamination from star-forming galaxies: in their large spectroscopic sample, Baldwin et al. (1981) found no [H II] region with detectable [Ne v], although some rare exceptions are known today (Izotov et al. 2004). Therefore, [Ne v] provides a powerful diagnostic tool in detecting AGN (Schmidt et al. 1998; Gilli et al. 2010).

In this paper we report on the first statistical optical sample (a total of 94 objects included in our type 2 AGN class) of [Ne v]-selected AGN found in spectra taken in the zCOSMOS Survey (Lilly et al. 2007). Throughout the paper, we adopt a "concordance" cosmology, $\Omega_{\rm M} = 0.25$, $\Omega_\Lambda = 0.75$, and $h = 0.7$. Magnitudes are given in the AB system.

## 2. The zCOSMOS-Bright spectroscopic survey

The Cosmic Evolution Survey (COSMOS, Scoville et al. 2007) provided superb angular resolution and depth with single-orbit $I$-band HST-ACS exposures over a two square degrees equatorial field (Koekemoer et al. 2007), along with deep ground-based images with excellent seeing (Capak et al. 2007). The zCOSMOS spectroscopic survey (Lilly et al. 2007) yields spectroscopic redshifts for a large number of galaxies in the COSMOS field using VIMOS, a multi-slit spectrograph mounted on the 8 m UT3 of the European Southern Observatory's Very large Telescope (ESO VLT). The zCOSMOS redshift project has been designed to efficiently use VIMOS by splitting the survey into two parts: first, the zCOSMOS-bright is a purely magnitude-limited survey, which has spectroscopically observed about twenty thousands objects brighter than $I = 22.5$ across the entire COSMOS field, with a medium-resolution grism ($R \sim 600$) and over a red spectral range (5500–9700 Å). This selection culls galaxies mainly in the redshift range $0.1 < z < 1.2$. The second part, zCOSMOS-deep, has targeted about 10 000 $B < 25$ galaxies, selected within the central 1 deg$^2$, using color-selection criteria to encompass the redshift range $1.4 < z < 3.0$. In this case, observations were performed with the $R \sim 200$ LR-Blue grism, which provides a spectral coverage from 3600 to 6800 Å. Because of the spectral and redshift ranges covered, the vast majority of the zCOSMOS-deep spectra sample a rest-frame wavelength interval shortward of 3000 Å. Thus, in this paper we used only the zCOSMOS-bright spectra in the search for the [Ne v] $\lambda$3426 emission line. The spectra were reduced and calibrated with the VIMOS Interactive Pipeline Graphical Interface software

(VIPGI, Scodeggio et al. 2005), while the redshift measurements were obtained with the help of an automatic package (EZ, Garilli et al. 2010) and were then visually checked. For more details about the zCOSMOS survey, we refer to Lilly et al. (2009).

## 3. [Ne v]-selected samples

### 3.1. Sample selection

The 20k zCOSMOS-bright sample (hereafter the zCOSMOS sample) has been built from a magnitude-limited survey, with a fairly high sampling rate (≈70%) and well-understood completeness properties (Zucca et al. 2009), which makes it well-suited for statistical studies of AGN. Among the 20707 entries included in the zCOSMOS spectroscopic catalog (version 4.2), a total of 18141 galaxies and AGN have measured redshifts, 1031 objects (5%) are spectroscopically classified as stars, and 1535 objects (7%) remain without redshift identification. Of course, the success rate in securing a redshift is a function of the redshift itself, the rest-frame color and the magnitude, but Lilly et al. (2009) showed that it is very high (≈95%) for the zCOSMOS sample between $0.5 < z < 0.9$. To guarantee that both the [Ne v] $\lambda$3346 and [Ne v] $\lambda$3426 emission lines fall within our spectral coverage, we limited our analysis to redshifts higher than 0.65. The standard zCOSMOS redshift measurement process includes several interactive steps in which broad-line AGN were identified and flagged; initially, we excluded the previously identified type 1 AGN from our analysis, because our principal aim is to collect a sample of obscured AGN. The analyzed sample contains 7624 galaxies with redshifts between 0.65 and 1.50, and the corresponding 8188 spectra[1] were visually inspected and measured to identify the [Ne v]-emitting objects.

The careful [Ne v]-selection procedure consisted of two main steps. First, all galaxy spectra were smoothed with a three-pixel boxcar and were plotted in the rest frame, to detect the [Ne v] $\lambda$3426 feature in emission with a semi-automatic procedure adapted from the IRAF task *splot* and to compile a list of candidate AGN. This supervised but automatic preliminary analysis, which identified a possible [Ne v] emission line only if its peak was above 2.5 times the significance level as derived by the noise of the surrounding continuum and its center was within ±20 Å of the expected position, reduced the number of galaxies to be examined in more detail to a few hundreds. The final phase of the selection process consisted of a careful examination of the one- and two-dimensional sky-subtracted spectra to eliminate the spurious detections (sky-line residuals, cosmic-rays residuals, zero-order contaminations); to mark as secure candidates galaxies where both [Ne v] emission were lines clearly visible at the expected positions; and to accurately verify the reliability of the [Ne v] $\lambda$3426 lines when the three times fainter [Ne v] $\lambda$3346 feature was not detectable. Following this laborious but accurate selection, we identified 95 zCOSMOS galaxies with a secure detection of [Ne v] in their spectra. The permitted narrow emission lines visible in the observed spectral range of these galaxies (i.e., Mg II, H$\gamma$, and H$\beta$) were analyzed to investigate the possible presence of a faint broad component. We found no broad component in any spectrum of the [Ne v]-selected objects, and we estimated an upper limit to the flux ratio of the narrow and broad components of about 10–20%, depending on the emission-line intensity and continuum signal-to-noise ratio (S/N). Given these spectral properties, we can confidently classify all selected objects as type 1.9–2 AGN; hence the 95 galaxies constitute our bona-fide obscured AGN sample.

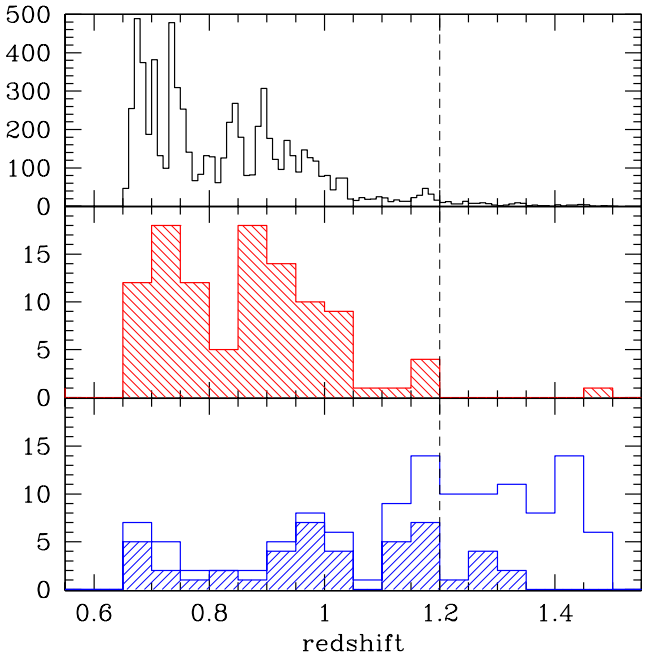


**Fig. 1.** Redshift distributions of zCOSMOS extragalactic objects in the redshift range examined ($0.65 < z < 1.50$). *Top panel*: parent galaxy sample. *Middle panel*: narrow-emission-line galaxies with [Ne v] detection. *Lower panel*: broad-line AGN selected from the zCOSMOS survey (empty histogram); the hatched histogram shows the [Ne v]-detected objects. The vertical dashed line marks the upper redshift limit at $z = 1.2$.

In the redshift range where the [Ne v] falls within our spectral coverage, the zCOSMOS survey discovered 112 broad-line AGN. We applied the same analysis to this type 1 AGN sample, detecting the [Ne v] emission line in 45 objects (40%).

The redshift distributions of our AGN samples, along with that of the parent galaxy population, are presented in Fig. 1. The redshift distribution of the [Ne v]-selected emission line galaxies (the type 2 AGN sample; middle panel) clearly follows that of the zCOSMOS galaxies, with a steady decline at redshifts greater than ∼0.9 and then an almost complete lack of objects above $z = 1.2$, with a single noteworthy exception at $z = 1.45$. The reason for the paucity of [Ne v]-detected objects in the highest redshift interval is twofold: first, the magnitude-limited zCOSMOS survey naturally selected normal galaxies as well as obscured host-dominated type 2 AGN up to $z \sim 1.2$ (Le Fèvre et al. 2005; Lilly et al. 2007). Second, at redshifts greater then 1.2, the [Ne v] feature enters the wavelength region where the zCOSMOS spectra are severely affected by fringing, making it more difficult to detect the emission line over the noisy continuum. As a confirmation of this effect, we can look at the type 1 AGN sample, which was not selected on the basis of [Ne v]-detection: at $z \leq 1.2$, the fraction of broad line objects with a detected [Ne v] emission line is 62% (37/60), whereas the ratio drops to a mere 13% (7/52) among objects with $z > 1.2$. Because of the difficulties in identifying [Ne v]-selected AGN above this redshift threshold, we limited the redshift interval to $0.65 < z < 1.20$, drawing two final samples of 94 narrow-line (type 2) and 60 broad-line (type 1) AGN.

[1] In the 20k zCOSMOS sample more than 5% of the targets were observed twice or more (see Lilly et al. 2009).

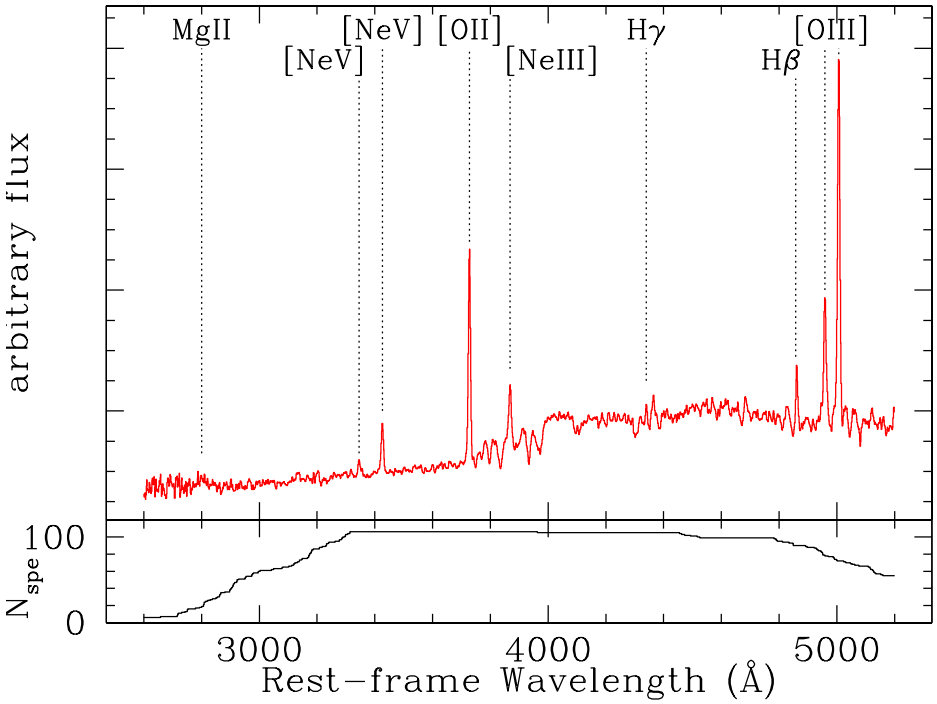


**Fig. 2.** Composite spectrum of the type 2 AGN sample with identification of the main emission lines. The flux is given per unit wavelength ($F_\lambda$) and the normalization is arbitrary. The number of single spectra contributing to the composite is shown in the bottom panel as a function of the rest-frame wavelength.

### 3.2. Type 2 vs. type 1 samples

In this section we compare the mean optical properties of the two AGN samples, the [Ne v]-selected type 2 sample and the type 1 sample, the latter selected on the sole basis of the presence of a broad component in the emission lines visible in the spectra (hereafter NL- and BL-samples). First, we generated composite spectra for each AGN class by averaging all available zCOSMOS spectra included in that class. To create the composite, each spectrum was shifted to the rest-frame according to its redshift (with a 1.5 Å rest-frame bin[2]) and normalized to a common wavelength range, which is always present in the observed spectral window. An identical weight was assigned to each individual spectrum to avoid biasing the final composite toward the brightest objects.

In Fig. 2 the average spectrum, obtained by stacking the spectra of ninety-four [Ne v]-detected galaxies, is plotted. It clearly shows strong, high-ionization narrow lines, in particular those of neon, but a very faint Mg II emission line. In Fig. 2 the main emission lines visible in the rest-frame spectral range covered by the observations are also labeled, while a summary of the principal emission line parameters is presented in Table 1. Indeed, the type 2 sample composite spectrum closely resembles the spectrum of a Seyfert 2 galaxy, although the line ratios would place it in the transition region of the diagnostic diagram involving the blue emission lines ([O III]$\lambda$5007, H$\beta$, and [O II]$\lambda$3727; Lamareille et al. 2004), commonly used at these redshifts. All emission lines are unresolved (the upper limit of 700 km s$^{-1}$ roughly corresponds to the spectral resolution of the zCOSMOS data), with the possible exception of the [Ne v] line itself, which seems marginally resolved, and of the very faint Mg II feature. But in the latter case the low S/N of the line prevents us from obtaining a reliable FWHM estimate.

To obtain accurate flux measurements of the narrow Balmer emission lines in the spectral range, we used Bruzual & Charlot (2003, BC03) population synthesis models to fit and subtract the stellar continuum in the composite spectrum of the type 2 AGN; the fitting procedure allowed us to account for the underlying stellar absorption of the Balmer lines. The mean optical extinction in the narrow-line region (NLR), derived from the observed H$\beta$/H$\gamma$ flux ratio, is quite low ($\langle E(B-V)\rangle = 0.18$). This is expected, since the AGN obscuration occurs in the inner core of the galaxies, and a significant amount of dust in the NLR would have prevented us from detecting the blue [Ne v] emission line. The absorption-line continuum of the composite could also provide useful information about the average stellar content of the galaxies hosting our type 2 AGN sample. A set of 39 BC03 template spectra, spanning a wide range in age and metallicity, were used to fit the emission-line-free regions of the composite. The best-fit model corresponds to an old stellar population with an exponentially declining star-formation, with ratio between galaxy's age and SF e-folding time of $t/\tau \approx 2$. These model parameters

**Table 1.** Spectral measurements in AGN composite spectra.

| | NL-AGN | | BL-AGN ([Ne v]-det.) | | BL-AGN (no-[Ne v]) | |
|---|---|---|---|---|---|---|
| Line | *EW* [Å] | *FWHM* [km s$^{-1}$] | *EW* [Å] | *FWHM* [km s$^{-1}$] | *EW* [Å] | *FWHM* [km s$^{-1}$] |
| Mg II$\lambda$2800 | 6.2 | | 42.0 | ~5000 | 64.0 | ~7500 |
| [Ne v]$\lambda$3346 | 2.3 | | 0.9 | | 0.6 | |
| [Ne v]$\lambda$3426 | 8.2 | ~900 | 3.1 | ~1000 | 1.4 | ~1100 |
| [O II]$\lambda$3727 | 29.3 | <700 | 7.0 | <700 | 12.8 | ~900 |
| [Ne III]$\lambda$3869 | 6.0 | <700 | 3.5 | <700 | 3.1 | <700 |
| H$\gamma$ | 3.2 | <700 | 8.6 | ~2500 | 3.8 | ~2000 |
| H$\beta$ | 8.2 | <700 | 21.4 | ~2000 | 22.0 | ~2000 |
| [O III]$\lambda$4959 | 9.0 | <700 | 6.9 | <700 | 4.2 | ~800 |
| [O III]$\lambda$5007 | 33.2 | <700 | 20.5 | <700 | 13.1 | ~800 |

**Notes.** All values are rest-frame values. H$\gamma$ is severely contaminated by the adjacent [O III] $\lambda$4353 line in BL-AGN composite spectra. The FWHM of low S/N emission lines is highly uncertain, and its value is missing in the table; FWHM upper limits refer to unresolved emission lines.

[2] At the median redshift of the analyzed galaxy sample ($z \sim 0.82$), a rest-frame bin of 1.5 Å matches the pixel size of the observations.

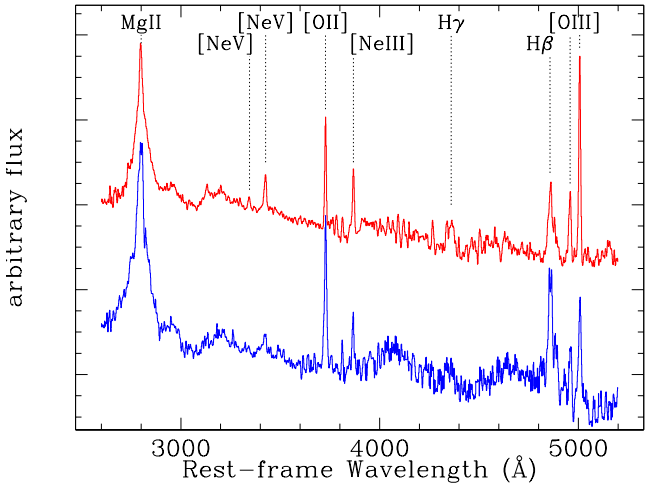


**Fig. 3.** Average spectra of the type 1 AGN samples with the identification of the main emission lines: the lower composite spectrum (in blue) represents the type 1 sample without [Ne v] detection, while the upper composite spectrum (in red) is the average of the [Ne v]-detected type 1 AGN; the spectra are offset for clarity. The flux is given per unit wavelength ($F_\lambda$), and the normalization is arbitrary.

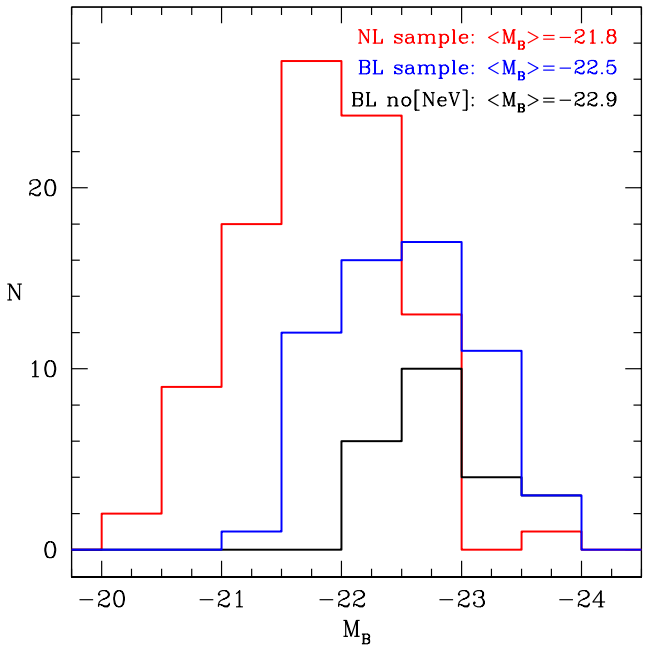


**Fig. 4.** Absolute *B*-magnitude distributions: the red histogram represents the sample of 94 type 2 AGN, the blue histogram the sample of 60 type 1 AGN, and the black histogram the subsample of 23 BL-AGN with undetected [Ne v]. The median absolute *B*-magnitudes of the three samples are also indicated.

roughly approximate a galaxy of Hubble-type Sa/Sb (Buzzoni 2005).

We also computed the average spectra of type 1 AGN by stacking spectra of the thirty-seven broad-line AGN with a [Ne v] detection and the twenty-three objects without a detectable [Ne v] line. The two composite spectra are presented in Fig. 3 and are clearly similar. Nevertheless, looking at Table 1, where the principal emission line parameters are listed, it is possible to identify the main difference: the H$\beta$/H$\gamma$ flux ratio in type 1 AGN without [Ne v] emission is significantly higher than in [Ne v]-detected ones, suggesting a larger mean optical extinction in the corresponding subsample. The higher average extinction in the sample 23 BL-AGN without [Ne v]-detection could explain why this feature is missing in the individual spectra, but is visible in the high S/N stacked spectrum.

The non-detection of the [Ne v] emission line in a fraction of type 1 AGN spectra is probably also related to the stronger continuum emerging from the central engine in these objects, which is shielded in the NL-sample. In support of this hypothesis, the absolute B-magnitude distributions of the AGN samples are presented in Fig. 4. Absolute magnitudes were computed following the method described by Ilbert et al. (2005), using a set of templates for the K-correction and all the available photometric information. To reduce the importance of the K-correction assumption, the rest-frame absolute magnitude was derived using the apparent magnitude from the closest (depending on the redshift) observed band. In Fig. 4 a clear trend is visible: the median absolute *B*-magnitudes in the three sample distributions are –21.8, –22.5, and –22.9, for the total NL-sample, the total BL-sample, and the subsample of unobscured AGN with undetected [Ne v] respectively. It is indeed expected that the NL-sample is composed of less luminous objects than the unobscured AGN, which belong to the BL-sample, but the higher luminosity of the BL-AGN with undetected [Ne v] corroborates the idea that the detection of this faint spectral feature becomes more difficult when the (unobscured) nuclear continuum increases. A more detailed analysis of the type 2 sample completeness, in terms of [Ne v] line detection, is discussed in the next section.

Finally, we compare the properties of the average spectrum of our BL-sample with those of the SDSS quasar composite (Vanden Berk et al. 2001): the broad Mg II line equivalent width (EW) is significantly larger on average in our AGN sample than observed in the more luminous SDSS quasars ($EW$ = 32 Å; see Table 2 in Vanden Berk et al. 2001). This is expected in the framework of the Baldwin effect (Baldwin 1977, but see also the thorough discussion of the observational biases in Zamorani et al. 1992). Conversely, the H$\beta$ relative intensity is lower in our composite spectra than in the SDSS spectrum ($EW \approx 22$ Å and 46 Å, respectively), and the continuum is significantly redder. These results are consistent with the hypothesis that in the red part of the rest-frame optical range, our composite spectra are significantly contaminated (and reddened) by the host galaxy stellar light. Very similar results were obtained by Gavignaud et al. (2006), who selected their type 1 AGN sample from the VVDS survey, a spectroscopic survey that shares many characteristics (magnitude limit, instrument) with zCOSMOS. Although a detailed study of the broad-line AGN component in the zCOSMOS survey is beyond the scope of this paper and will be addressed in a future work, the preliminary analysis presented above indicates that the zCOSMOS BL-samples, both the [Ne v]-detected subsample and that without [Ne v], do not show atypical spectral properties compared with other known quasar samples.

### 3.3. Type 2 AGN sample completeness

The principal aim of this paper is to select and study a sample of obscured AGN at redshift ≈1. The BL-sample was collected mainly for comparison purposes. For this reason, our main concern is related to the efficiency of our detection technique in selecting narrow-line [Ne v]-emitting galaxies, after interpreting the incomplete detection of the [Ne v] emission line in type 1

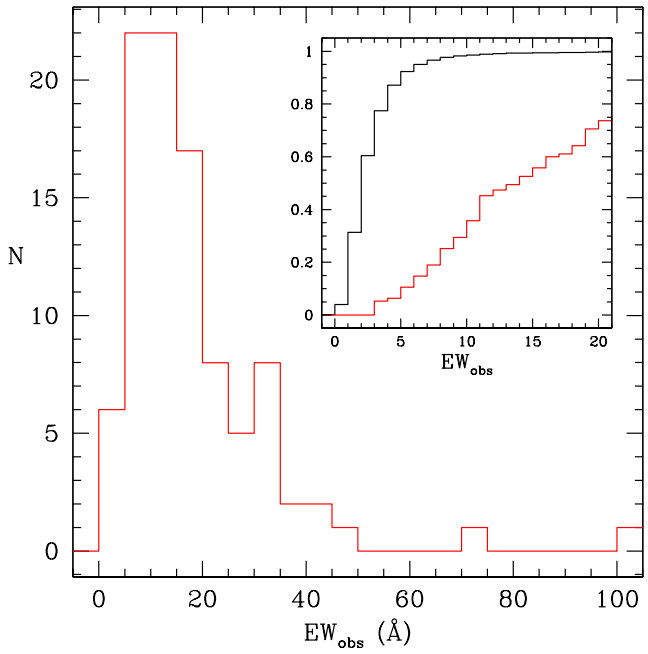


**Fig. 5.** Observed [Ne v] equivalent widths distribution of the sample of type 2 AGN. The inset shows (in red) the corresponding cumulative distribution of the detected [Ne v] emission lines, along with the cumulative distribution (in black) of the EW upper limits for the zCOSMOS galaxies without [Ne v] detection.

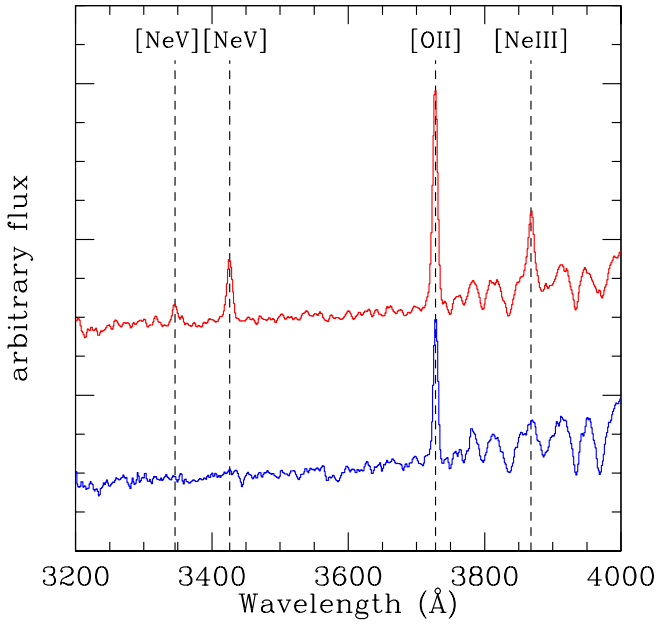


**Fig. 6.** Composite spectra of the [Ne v]-selected type 2 AGN sample (top, in red) and of the X-ray-emitting galaxies without [Ne v] detection (bottom, in blue); the spectra are offset for clarity.

objects as a combined effect of smaller emission line EWs and S/N in zCOSMOS spectra.

To support the effectiveness of our technique in selecting a fairly complete sample of type 2 AGN, at least in terms of [Ne v] emission, we analyzed the distribution of the detected line EWs, presented in Fig. 5. The observed EW distribution of the [Ne v] emission line is peaked at around 10 Å, with a long tail up to ≈100 Å. The inset of Fig. 5 shows the cumulative EW distribution of the detected [Ne v] lines, along with the cumulative distribution of the EW upper limits for the 7265 zCOSMOS galaxies with undetected [Ne v]. The detection limits were estimated from the S/N in the continuum adjacent to the line, following the procedure outlined by Mignoli et al. (2009) on the basis of a larger sample of emission-line galaxies drawn from the zCOSMOS survey. Comparing the two cumulative distributions, we find that 92% of the galaxies with undetected [Ne v] have upper limits lower than 5 Å, while only six type 2 AGN show EWs smaller than the same threshold. Since there is no reason to expect that galaxies with loose upper limits include a different percentage of AGN than the parent sample (1.3%), we can confidently conclude that our selection misses very few strong [Ne v] emitters (with an EW larger than ≈5 Å).

We also examined our detection efficiency by exploiting the multi-wavelength data set of the COSMOS field, using the Chandra-COSMOS Survey (C-COSMOS; Elvis et al. 2009) to pinpoint AGN candidates in X-rays. The sample of zCOSMOS galaxies without broad lines in their spectra and $0.65 < z < 1.20$ includes 5148 objects inside the Chandra mosaic; 180 of these galaxies have been associated with an X-ray source in the C-COSMOS catalog (details on the X-ray catalog and matching criteria can be found in Puccetti et al. 2009; Civano et al. 2012, and in Sect. 5.1). Most of these galaxies probably harbor an active galactic nucleus, since their X-ray luminosity is higher than $10^{42}$ erg/s, and it has been shown that other sources of X-ray emission in normal galaxies (i.e. high-mass binaries; Moran et al. 1999) cannot easily account for such high luminosities. We stacked 158 optical spectra of the X-ray emitting galaxies without [Ne v] detection using the same recipe as adopted for the [Ne v]-detected type 2 AGN sample; the two composite spectra are shown in Fig. 6. Visually comparing the two spectra, the complete absence of the [Ne v] doublet in these X-ray emitting galaxies is striking; an upper limit of 0.5 Å to the [Ne v] equivalent width can be obtained from the S/N of the continuum. Therefore, we can confidently assert that the selection process did not miss a significant number of galaxies with the [Ne v] emission line in the EW range of 1–3 Å, since such a population of weak [Ne v] emitters do not emerge even in a complementary X-ray-selected AGN sample. On the other hand, the significant number of X-ray-emitting galaxies, probably hosting an obscured AGN, without a detectable [Ne v] emission clearly indicates that this technique alone is not sufficient to select a complete sample of type 2 AGN. The mean optical extinction in these X-ray-emitting galaxies derived from the H$\beta$/H$\gamma$ flux ratio measured in their composite spectrum is $\langle E(B-V)\rangle = 0.27$, higher than in the [Ne v]-selected type 2 AGN sample, suggesting dust extinction on galactic or NLR scale as a possible cause for the [Ne v] paucity in these objects.

## 4. [Ne v]-selected type 2 AGN sample properties

### 4.1. Stellar mass distribution of the host galaxies

Stellar masses were computed by Bolzonella et al. (2010) for both the type 2 AGN and galaxy parent samples. Briefly, they used different stellar population synthesis models to fit the large set of optical and near-infrared photometry available in the COSMOS field, using a $\chi^2$ minimization to find the best-fit model, at a fixed redshift $z = z_{spec}$ from the zCOSMOS survey. More details on stellar mass determination can be found in Bolzonella et al. (2010) and Pozzetti et al. (2010).

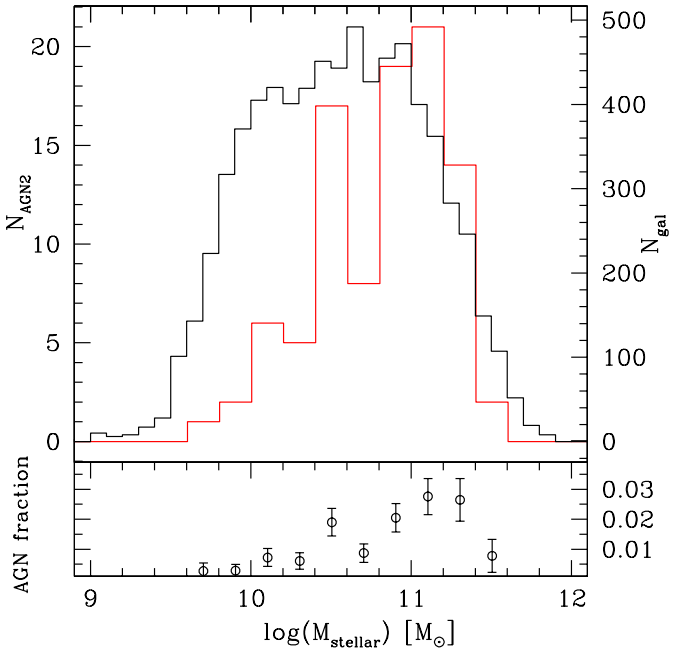


**Fig. 7.** Host stellar mass distribution for the type 2 AGN sample (red histogram) compared with that of the galaxy parent sample (black histogram; $0.65 < z < 1.20$). The $y$-axes used for the two histograms are scaled relative to each other to facilitate the comparison. In the *bottom panel*, the ratio between the two populations is shown.

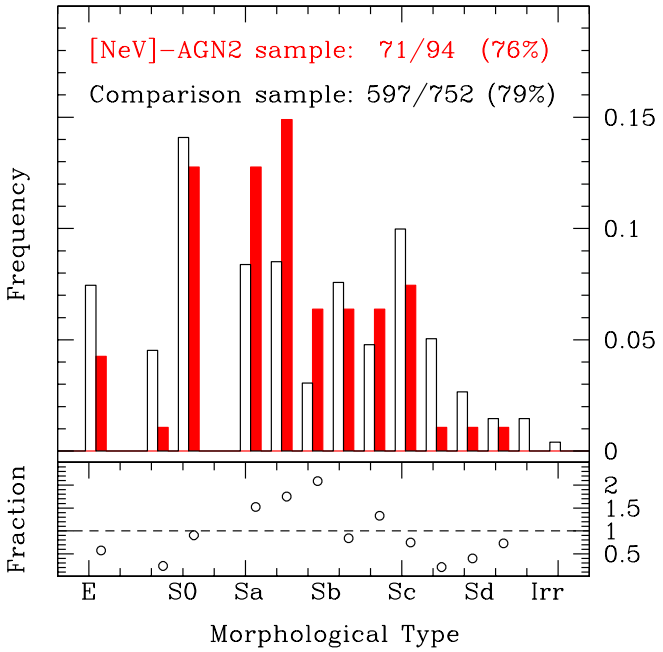


**Fig. 8.** Morphology distribution of the 71 classified type 2 AGN hosts (red filled histogram) compared with that of the 597 normal galaxies belonging to the control (8×) mass-matched sample (black empty histogram). In the bottom panel, the fraction between the relative frequencies of the two populations is plotted as a function of the Hubble types.

Previous studies of type 2 AGN host galaxy properties have assumed that the contamination of the AGN light to their stellar masses measurements is negligible (Silverman et al. 2008; Schawinski et al. 2010). Bongiorno et al. (2012) analyzed the differences between the stellar masses computed using SED fitting with only a galaxy component and those obtained with two components (AGN and galaxy). They applied the two SED fittings to a large sample of AGN in the COSMOS field: our [Ne v]-selected AGN, included in their work, shows the least differences in the computed stellar masses between the various AGN classes, with a median of mass ratios $M_{(\mathrm{gal})}/M_{(\mathrm{gal+AGN})} = 1.04$. Our [Ne v]-selected type 2 AGN sample is composed of galaxies hosting relatively low-luminosity and obscured AGN, so we can confidently compare their derived properties with those of the parent sample.

Figure 7 shows the stellar mass distribution of galaxies hosting the type 2 AGN sample (red histogram) along with that of the parent galaxy sample (black histogram). From the top panel of Fig. 7, we can see that the stellar mass for most type 2 AGN hosts is in the range $1 \times 10^{10}$–$3 \times 10^{11}$ $M_{\odot}$, while the galaxies of the parent sample have masses down to $5 \times 10^{9}$ $M_{\odot}$. The median stellar mass of the type 2 AGN host galaxies is $8 \times 10^{10}$ $M_{\odot}$, while for the parent galaxy sample it is $3.7 \times 10^{10}$ $M_{\odot}$. We used a two-populations Kolmogorov-Smirnov (K-S) test to assess the significance of the difference between the masses of the parent sample and the AGN host galaxies, finding that they differ at very high significance ($>5\sigma$).

The fraction of [Ne v]-selected obscured AGN in our zCOSMOS sample is shown as a function of the host stellar mass in the lower panel of Fig. 7, with the percentage of type 2 AGN rising from less than 1% at $\sim 2 \times 10^{10}$ $M_{\odot}$ to around 3% at $\sim 2 \times 10^{11}$ $M_{\odot}$. A similar trend is shown by purely X-ray-selected AGN in zCOSMOS (Silverman et al. 2009), and in larger X-ray sample (Aird et al. 2012), although we show below that the two selection techniques ([Ne v] and X-ray) are more complementary than overlapping. In optically selected AGN samples the detection rate is also strongly dependent on host galaxy mass, as established in a sample of SDSS emission-line galaxies (Kauffmann et al. 2003).

### 4.2. Morphologies of the host galaxies

To compare the morphologies of our AGN host galaxies with those of normal galaxies, we built a control sample of galaxies from the zCOSMOS survey. Given the different mass distribution highlighted in Fig. 7, for each of the 94 narrow-line AGN we selected 8 galaxies from the parent sample with matched redshift and stellar mass. We made use of the morphological catalog by Nair et al. (in prep.) that, using the F814W-band images from the Advanced Camera for Surveys (ACS) available in COSMOS and following the method applied in Nair & Abraham (2010), visually classifies all galaxies belonging to zCOSMOS, and divides them into different types (Ell, S0, Sa-Sd, and Irr). A clear classification into one of the Hubble types was possible for 71 out of 94 (76%) of the AGN host galaxies, while a similar fraction of galaxies (597/752, 79%) were classified in the control sample. The objects without an assigned regular morphology are mainly of two classes: for some galaxies, the resolution and S/N is such that it was not possible to establish an accurate morphological type, but the majority of the unclassified objects shows peculiar morphologies (doubles, tadpoles, and chain galaxies) and do not find a natural place in the Hubble sequence.

The AGN host galaxy morphology distribution is plotted along with that of the control sample in Fig. 8, where only objects with assigned Hubble type are shown. The two distributions are not strikingly different, since the significance of the difference between the two populations is at about $2\sigma$ level, as estimated from a K-S test. Even if the two distributions are similar,

the lower panel of Fig. 8 seems to suggest a difference in the trend of the relative frequency of the Hubble types: the hosts of the [Ne v]-selected type 2 AGN prefer the early-spiral morphologies (Sa-Sb), with an expected paucity of late-spirals and irregulars, but also with a lower fraction of elliptical galaxy hosts than the control sample.

### 4.3. Optical spectroscopic properties

We measured the [Ne v] and [O ii] emission lines in all available zCOSMOS spectra of the AGN included in the type 1 and type 2 samples selected by [Ne v]-detection. We used a semi-automatic procedure that exploits the IRAF task *splot*: first, the continuum was automatically fitted to fixed wavelength intervals, although our procedures also enabled interactive adjustments of the continuum level to improve the line measurement in noisy spectra. Then, EWs and fluxes were measured by applying a Gaussian-function fitting algorithm of the continuum-subtracted line profiles. The measurement errors, estimated from the rms of the continuum close to the line after the Gaussian fit is subtracted, are about 5–10% for the [O ii], and 10–20% for the fainter [Ne v]. Moreover, repeated observations exist for more than 5% of the zCOSMOS sample, and spectral measurements obtained from these repeated spectra are consistent within the errors quoted above.

We investigated the [O ii]/[Ne v] line-flux ratio in our [Ne v]-selected samples of broad- and narrow-line AGN. According to the unification model (Antonucci 1993), the NLR emission properties should be similar in both AGN types. Thus, under the hypothesis that the [Ne v] emission and NLR [O ii] component are linked, a higher line-flux ratio in the obscured population, with respect to typical type 1 AGN values, would favor the scenario of enhanced star formation in type 2 AGN invoked by semi-analytic models of galaxy formation and evolution (Gilli et al. 2010, and references therein).

The mean (median) flux ratio is 4.05 (3.13) in the NL sample and 2.10 (1.62) in the BL sample. Because of different selection efficiencies in the two samples (see Sect. 3.2), we also extracted a subsample with redshift and [Ne v] flux distributions matching those of the BL-AGN from the larger sample of NL-AGN. Again, the mean (median) [O ii]/[Ne v] intensity ratio is 4.14 (3.51) in this BL-matched type 2 AGN sample. We measured the flux ratio also in the composite spectra of type 2 AGN and [Ne v]-detected type 1 AGN samples presented in Sect. 3.2, obtaining similar values of 3.62 and 1.94, respectively. The composite spectrum of the type 2 AGN sample, selected at redshifts $0.3 < z < 0.83$ from the Sloan Digital Sky Survey, shows an intensity ratio that agrees well with the averages measured in this work ($4.5 \pm 0.3$; Zakamska et al. 2006). The significantly higher value of the [O ii]/[Ne v] flux ratio is therefore suggestive of enhanced star formation for a given [Ne v] luminosity in the obscured population, at least with respect to the sample of type 1 AGN.

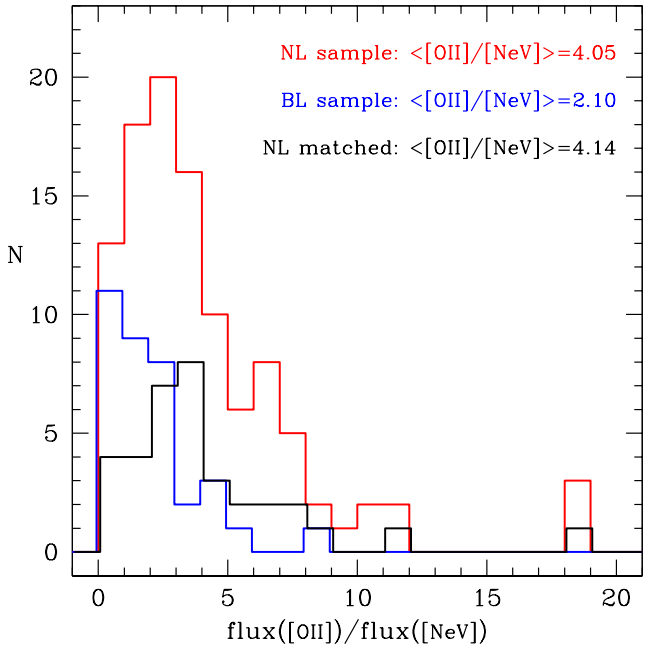


**Fig. 9.** [O ii]/[Ne v] line-flux ratio distributions: the red histogram represents the sample of type 2 AGN, the blue histogram the sample of type 1 AGN with detected [Ne v], and the black histogram the subsample of NL-AGN that match the redshift/flux characteristics of the BL-AGN. The average flux ratios of the three samples are also indicated.

## 5. Comparison with other type 2 AGN selection techniques at $z \sim 1$

The cosmological evolution of unobscured quasars has been relatively well studied out to very high redshifts ($z \sim 5$–6) thanks to large optical surveys, mostly the 2dF QSO Redshift Survey (Croom et al. 2004) and the Sloan Digital Sky Survey (SDSS; Richards et al. 2006); on contrary, there are not many samples of optically selected, high-$z$ type 2 AGN available in the literature, and their space density beyond the local universe is poorly known. The selection of complete samples of obscured AGN is a difficult task, and the two methods commonly regarded as the most complete, the optical emission line selection and the X-ray detection, have their own biases. In the optical, dust extinction throughout the host galaxy can significantly reduce the observed emission line luminosity and/or alter the line ratios. Moreover, the emission line selection suffers from a redshift-dependent completeness, since at different redshifts the diagnostic diagrams exploit different line ratios, with different efficiencies and specificities. On the other hand, the X-ray selection, while largely unaffected by extinction in the host galaxy, is biased against sources in which nuclear emission is absorbed by Compton-thick gas close to the central engine.

Consequently, the type 2 AGN detection rate strongly depends on the adopted selection criteria and sample definition. There is no single known method that can select a complete sample of obscured AGN, and we are not aware of any selection technique capable to identify all objects found by other methods. In this section, we compare the result of our [Ne v]-selection technique with other AGN selection methods, using as reference the parent sample of 7358 galaxies with $0.65 < z < 1.20$ and $I < 22.5$, selected from the zCOSMOS Redshift Survey.

### 5.1. X-ray selection

The sample of zCOSMOS galaxies without broad lines in their spectra and redshift range $0.65 < z < 1.20$ includes 5148 objects within the Chandra mosaic; 180 of these galaxies show X-ray emission (all above $10^{42}$ erg s$^{-1}$) and are very likely obscured AGN. Only 23 [Ne v]-selected sources are detected by Chandra within 1.2 arcsec from the optical position; the median distance between the X-ray and optical counterpart is 0.46 arcsec. To derive rest-frame, observed (i.e., prior to absorption correction)

2–10 keV fluxes, we extracted the X-ray counts for these sources using the multiple pointings of the Chandra-COSMOS mosaic. Here we present a summary of the adopted procedure; a more exhaustive description will be presented in a forthcoming paper (Vignali et al., in prep.).

Because of the tiling strategy in the C-COSMOS field, every source can be observed in more than one pointing and at different locations within the ACIS-I field-of-view, hence the source count distribution is generally characterized by different PSF sizes and shapes. To properly account for all of these effects, we used the Acis Extract software (Broos et al. 2010), which extracts the source counts from each observation using the 90% of the encircled energy fraction at 1.5 keV at the source location and then correcting for aperture. X-ray photometry in the observed band corresponding to the rest-frame 2–10 keV band was then converted into a count rate using the exposures derived from the time maps at each source position, and then into a flux assuming a power-law with photon index $\Gamma = 1.4$. To provide support to our results, X-ray spectra were also extracted for all of the 23 sources and fitted using XSPEC (version 12.6; Arnaud 1996) with a a power-law modified by Galactic absorption only. The derived rest-frame 2–10 keV fluxes were found to be consistent, within their admittedly large errors, with the fluxes obtained by the simple count-rate-to-flux conversion described above.

For 46 of the remaining 48 [Ne v]-selected sources[3] without an individual X-ray detection, we derived upper limits to the X-ray flux with the same procedure as described above: at each source position, counts were extracted taking into account the PSF size and shape in the observed band equivalent to the rest-frame 2–10 keV energy range. One-sigma count upper limits were then converted into count rates using the time maps, which were finally converted into X-ray flux upper limits assuming a power-law with photon index $\Gamma = -0.4$, which is broadly consistent with a Compton-thick spectrum.

As a final remark, we note that the population traced by X-ray-detected [Ne v]-selected sources represents a limited fraction of the overall, very likely obscured, AGN population with an X-ray counterpart and no broad emission line in the optical spectra (23/180, i.e. 12.7%). The X-ray selection allows us to collect a larger number of $z \approx 1$ type 2 AGN than the [Ne v]-detection technique (180 vs. 71). Both samples include a population of heavily obscured AGN, as suggested by the distribution of column density for type 2 AGN in the Chandra-COSMOS survey (Lanzuisi et al. 2013) on the one hand and by the large fraction of X-ray-undetected [Ne v]-selected sources (48/71) on the other hand. In other words, the selection based on the lack of broad optical emission lines coupled to relatively strong ($>10^{42}$ erg s$^{-1}$) X-ray emission is somehow complementary to the selection of AGN based on the presence of [Ne v] emission.

### 5.2. Blue diagnostic diagram

The classical method for classifying star-forming galaxies and narrow-line AGN with optical spectroscopy is based on emission-line ratio diagnostics. The most efficient and commonly used BPT diagram requires two sets of line ratios: [N II] $\lambda$6583/H$\alpha$ and [O III] $\lambda$5007/H$\beta$. Unfortunately, in the redshift range of interest here, the H$\alpha$ line is outside the observed spectral range, so we need to rely on a diagnostic diagram based only on emission lines observed in the blue part of the optical spectra: [O III] $\lambda$5007, H$\beta$ and [O II]$\lambda\lambda$3726,3729. Such a diagnostic diagram (hereafter "blue diagnostic diagram"), recently applied to a smaller (10k) sample of zCOSMOS galaxies (Bongiorno et al. 2010), is less effective than the lower redshift, classical BPT diagnostic diagram. The emission line fluxes of the zCOSMOS galaxies were measured using the automated pipeline *platefit_vimos* (Lamareille et al. 2009), which simultaneously fits all emission lines with Gaussian functions after removing the stellar continuum. We checked the consistency of the platefit measurements with the [O II] fluxes measured by us in the sample of [Ne v]-selected AGN, finding an excellent agreement: the mean of the intensity ratio distribution was 0.997 and two flux measurements never differed by more than 20%.

The sample of zCOSMOS galaxies in the redshift range $0.65 < z < 0.92$ includes 5662 objects; this number includes 63 out of 94 [Ne v]-selected type 2 AGN. The upper redshift limit was chosen to ensure that the [O III] line is still within the observed spectral range. The basic requirement for a reliable classification is that all diagnostic emission lines are detected above a minimum S/N. In particular, we selected emission-line galaxies in the explored redshift range for which all lines are detected with $S/N > 3$. This S/N cut reduces the number of analyzed galaxies down to 2461 (43%), with the strongest criterion being that on H$\beta$, which is generally the weakest of the involved emission lines. A higher percentage (48/63; more than 75%) of [Ne v]-selected type 2 AGN satisfies the requirements for being included in the diagnostic diagram shown in Fig. 10. This diagram allows us to separate the zCOSMOS star-forming galaxies from the Seyfert 2-like objects that inhabit the upper part of the line ratio plane. The demarcation line, proposed by Lamareille (2010), separates the underlying galaxy population in 159 type 2 AGN (6.5%) and 2302 SFG. The position of the [Ne v]-selected narrow-line zCOSMOS galaxies is also shown (red square dots) in Fig. 10: a significant fraction (29/48 or 60%) of type 2 AGN selected via [Ne v] fall in the star-forming region of the blue diagnostic diagram. Conversely, of the 159 type 2 AGN selected on the basis of their emission line ratios, only 19 (12%) show a detectable [Ne v] emission. As an additional check, we stacked the optical spectra of the remaining 140 type 2 AGN, selected by the diagnostic diagram, detecting a very faint [Ne v] emission line with a rest-frame EW of 0.7 Å. In Fig. 10 we also highlight the emission-line galaxies with an X-ray counterpart in the Chandra catalog (open star symbols): again, 55 out of 66 (83%) X-ray sources (with $L_{0.5-10\mathrm{keV}} > 10^{42}$ erg s$^{-1}$, thus likely type 2 AGN) fall in the region of star-forming galaxies. This means that the [Ne v]-selected and X-ray-emitting type 2 AGN share a similar classification percentage and position in the blue diagnostic diagram, suggesting a heavy incompleteness in the line-ratios technique used to select high redshift ($z > 0.5$) obscured AGN.

The lower efficiency in selecting AGN of the blue diagnostic diagram has previously been reported in literature (Bongiorno et al. 2010; Stasińska et al. 2006), with a number of possible explanations: first, because of the large wavelength separation between the [O III] $\lambda$5007 and H$\beta$ emission lines, their flux ratio is very sensitive to dust obscuration on a galactic scale, and adopting an EW ratio can only mitigate the effect, because of the differential extinction between the emission line region and the stellar continuum in the galaxy spectra. Another possible reason for the presence of type 2 AGN in the SFG region is that in these objects star formation and AGN activity coexist. This hypothesis is consistent with model predictions for the position of the composite AGN/SF in the optical diagnostic diagrams (Stasińska et al. 2006). This explanation seems more plausible for the [Ne v]-selected type 2 AGN that fall in the SFG region,

[3] For two sources, no reliable X-ray photometry could be obtained from the available data.

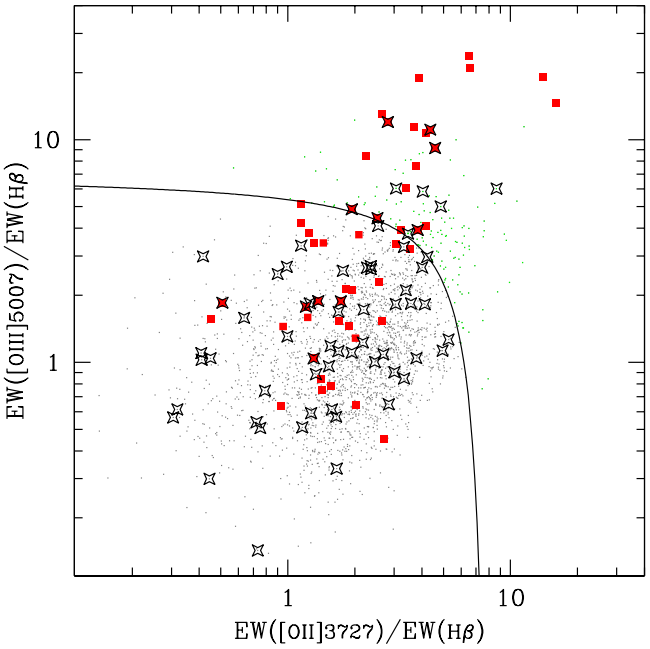


**Fig. 10.** Blue diagnostic diagram in the interval $0.65 < z < 0.92$. The solid line shows the demarcation between SFG and type 2 AGN defined by Lamareille (2010). Small points represent the 2461 zCOSMOS galaxies for which all emission lines are detected with an $S/N > 3$. Large red squares correspond to [Ne v]-selected objects, while the X-ray emitting galaxies are identified by large starred symbols.

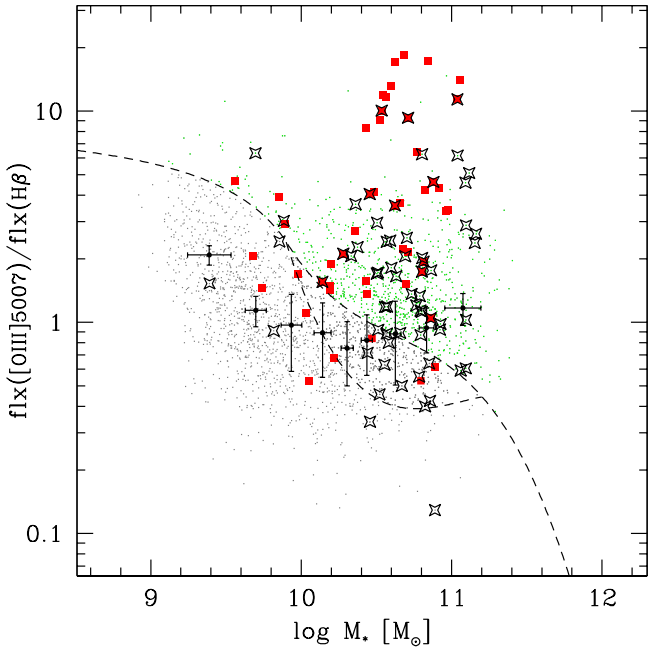


**Fig. 11.** Mass-Excitation (MEx) diagram in the redshift range $0.65 < z < 0.92$. The dashed lines show the empirical curves defined by Juneau et al. (2011), dividing the plane into an upper region, occupied by galaxies hosting an AGN, and a lower region where the star-forming galaxies are located. Objects located between the two curves are classified as AGN/SF composite galaxies. The small points represent the same sample of 2461 zCOSMOS galaxies used in Fig. 10. Large red squares correspond to [Ne v]-selected objects, while the X-ray emitting galaxies are identified by large starred symbols. The filled dots with error bars represent the line-flux ratios measured in nine composite spectra of galaxies that were not included in the diagram because of their low S/N emission lines. The horizontal error bars indicate the dispersion of the stellar mass values in each of the bin, whereas the vertical error bars show the estimated error on the flux ratios.

since a small amount of extinction in the host galaxy would erase the blue faint [Ne v] emission line.

### 5.3. Mass-Excitation (MEx) diagnostic

The Mass-Excitation diagnostic diagram has recently been proposed by Juneau et al. (2011) and offers, at $z \geq 0.5$, a more complete AGN selection than the optical blue diagram. It is derived from the classic BPT diagram, using the galaxy stellar mass as a surrogate for the [N II] $\lambda$6583/H$\alpha$ line ratio. Juneau et al. (2011) demonstrated that the MEx technique successfully distinguishes between star formation and AGN emission, also dealing with AGN/SF composite galaxies, the so-called MEx-intermediate class, which lie in a part of the diagram in between the AGN and SFG regions.

The same zCOSMOS galaxy sample adopted for the blue diagnostic diagram (objects in the range $0.65 < z < 0.92$ and with emission lines all detected with $S/N > 3$) was analyzed with the MEx diagnostic diagram presented in Fig. 11. The high efficiency in selecting AGN of the MEx technique is evident when looking at the position of the [Ne v]-selected (red squares) and X-ray emitting (starred symbols) type 2 AGN. A high percentage (39/48, more than 80%) of the [Ne v]-selected galaxies are classified as AGN, along with other four objects lying in the region of the diagram where AGN/SF composites are expected. Only five of them would be classified as star-forming galaxies by the MEx diagnostic diagram. Similarly, of the 66 X-ray emitting galaxies which satisfied the constraint for inclusion in the diagram, fifty are classified as AGN and eleven belong to the MEx-intermediate class. Once again, although the two samples have only a few objects in common, the [Ne v]-selected and X-ray-emitting type 2 AGN share an almost identical position and class percentage in the MEx diagnostic diagram.

However, a few words of caution about the efficiency of the MEx technique are appropriate. The inclusion of a very high percentage of AGN selected with other techniques is probably the consequence of a quite "generous" criterion for AGN classification by the MEx diagnostic. When it is applied to the zCOSMOS galaxies in the range $0.65 < z < 0.92$, about one-third of them (796) are classified as active, quite a large number of AGN compared with those identified by other techniques. Moreover, since more than 3000 galaxies are not included in the MEx diagram because of low S/N in their emission line measurements, we had to estimate how their removal would bias the AGN fraction. We divided the excluded galaxies into nine equally populated bins according to their computed stellar mass, and fluxes of the emission lines were measured in composite spectra. In seven of nine bins the value of [O III]/H$\beta$ flux ratio, plotted in Fig. 11 against the mean stellar mass, falls below the MEx empirical division curve, suggesting that zCOSMOS galaxies with low S/N spectra predominantly populate the star-forming region, and if they were included in the diagnostic diagram, the AGN percentage would decrease to $\approx$25%. In addition, since the empirical dividing lines used in Fig. 11 have been calibrated in Juneau et al. (2011) using a $z \sim 0.1$ SDSS galaxy sample, their application to our $z \sim 0.8$ sample should be taken with caution. Indeed, new computations carried out by Juneau et al. (in prep.) confirm that the loci of these diagnostic diagrams evolve with redshift, and that approximately 10% of the galaxies that fall in the AGN class when local relations are used are instead included in the SF region at

**Table 2.** Numbers of zCOSMOS emission-line galaxies classified as type 2 AGN by different selection techniques.

| | [Ne v] | X-ray | DD-Blue | DD-MEx |
|---|---|---|---|---|
| [Ne v] | **36 (2.1%)** | 11 (17%) | 12 (10%) | 30 (5.1%) |
| X-rays | 11 (31%) | **66 (3.9%)** | 11 (9.4%) | 50 (8.6%) |
| DD-Blue | 12 (33%) | 11 (17%) | **117 (6.8%)** | 69 (12%) |
| DD-MEx | 30 (83%) | 50 (76%) | 69 (59%) | **582 (34%)** |

**Notes.** The diagonal elements represent the number of galaxies classified as type 2 AGN by each technique, with corresponding efficiencies from the sample of 1712 galaxies for which all diagnostics are available. Type 2 AGN identified by two methods are shown as off-diagonal elements, along with the percentage from the total number of galaxies (boldface number in same column) selected by the specific diagnostic identified in the column top label.

$z = 0.7$. This would further decrease the MEx-AGN fraction in our zCOSMOS galaxy sample by a similar amount.

### 5.4. Relative efficiency of type 2 AGN selection techniques

In this section the previously discussed optical and X-ray diagnostics are compared. Since the different selection techniques are not applicable to all members of the parent galaxy sample, we extracted a subsample of 1712 galaxies (included in the Chandra field-of-view, with a redshift range of $0.65 < z < 0.92$, and with emission lines all detected with $S/N > 3$) for which all diagnostics are available to obtain a meaningful comparison. There are 651 objects that show at least one indication of activity, more than one-third of the galaxy population (38%) but, as already demonstrated in Sect. 5.3, excluding galaxies with low S/N emission lines in the MEx diagram may significantly increase the AGN percentage. If we do not take into account the MEx diagnostic, the AGN number drops to 191 (11%).

A relative evaluation of the techniques presented in this paper for selecting type 2 AGN at $z \approx 1$ can be drawn from Table 2: the first three selections ([Ne v] and X-ray detections, and the blue diagnostic diagram) are almost complementary, with a similar efficiency and relatively small overlaps, since the fraction of objects simultaneously detected by two methods ranges from 10 to 33%. Conversely, the MEx diagnostic seems highly efficient in selecting obscured active galaxies, since more than 50% of the type 2 AGN[4] identified by other methods are located in the AGN region of the MEx diagram. The differences in the nature of the selected type 2 AGN samples play an important role in the relative merits of the selection methods investigated. The [Ne v]- and X-ray-selected galaxies have a clear sign of nuclear activity, representing good single examples of powerful AGN. On the other hand, the MEx selection, with its probabilistic approach, produces a more complete *statistical* AGN sample, including also low-luminosity objects, but it can be affected by contamination especially when used on an object-by-object basis.

## 6. X-ray-to-[Ne v] flux ratio and the heavily obscured AGN content in zCOSMOS

Gilli et al. (2010) explored the potential of the observed 2–10 keV to [Ne v] emission-line luminosity ratio (X/NeV) as a method for discovering heavily obscured, possibly Compton-thick AGN up to $z \sim 1.5$. The zCOSMOS [Ne v]-selected type 2 AGN provide an ideal sample to apply this promising diagnostic.

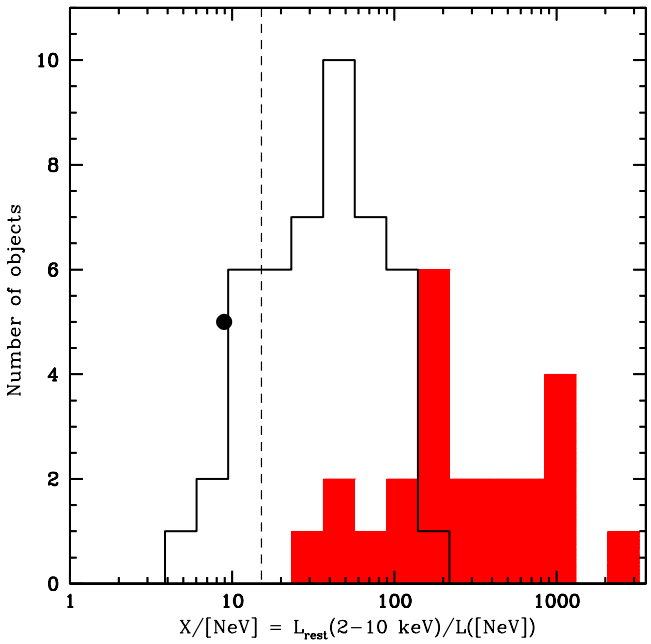


**Fig. 12.** Distribution of the observed (i.e., not corrected for absorption/extinction) rest-frame 2–10 keV to [Ne v] luminosity ratio (X/NeV) for the 69 zCOSMOS type 2 AGN with reliable X-ray photometry (23 X-ray detections and 46 upper limits, see Sect. 5.1 for details). The filled histogram represents the X-ray-detected objects, while the histogram delimited by the solid line shows the luminosity ratio upper limits for X-ray-undetected type 2 AGN. The vertical dashed line indicates the threshold defined by Gilli et al. (2010): objects to the left of this line are candidate Compton-thick AGN. The filled circle indicates the average value obtained from stacking the sample of 46 X-ray-undetected type 2 AGN.

To compare the [Ne v] line flux measured in zCOSMOS spectra with the integrated Chandra X-ray emission in a fair manner, we need to correct the optical spectral measurements for slit losses. In the redshift interval of interest ($z \geq 0.65$), the 1″-slit width used in zCOSMOS observations corresponds to a physical size greater than 7 kpc, so, unless the sizes of the NLR are unreasonably larger than the typical value of ≈1 kpc, the line flux that enters the spectrograph aperture can be considered as coming from a point source, and it is essentially affected by seeing variations only. Thus, we corrected the [Ne v] flux for each of our objects using aperture corrections estimated through spectroscopic stars observed in the same multi-slit mask of the analyzed AGN spectrum. In our type 2 AGN sample, the aperture corrections range between 0.03 and 1.69 mag, with a median value of 0.46 mag. Ten of the [Ne v]-selected galaxies had multiple zCOSMOS spectra, and applying the estimated aperture correction allowed us to lower the relative flux differences of the repeated measurements from 17% to 9% on average. The X-ray fluxes were computed in the 2–10 keV rest frame band and without any absorption correction to follow the definition given in Gilli et al. (2010).

The distribution of the X/NeV ratio for the 69 zCOSMOS type 2 AGN with reliable Chandra measurements (see Sect. 5.1 for details) is plotted in Fig. 12. Gilli et al. (2010) showed that

[4] Taking also in account the redshift evolution of the empirical dividing lines.

in a sample of local Seyferts, the AGN with X/NeV < 15 are almost all Compton-thick. In our [Ne v]-selected sample, nine type 2 AGN are below this threshold and are undetected in the X-rays. These sources can be safely considered robust Compton-thick AGN candidates. Of the 46 [Ne v]-selected type 2 AGN with X/NeV upper limits, 39 have X/NeV < 100, suggesting a column density possibly exceeding $10^{23}$ cm$^{-2}$ (Gilli et al. 2010). Conversely, all of the 23 X-ray-detected objects fall in the region that is probably populated mostly by Compton-thin AGN (with 30 < X/NeV < 2100).

Synthesis models of the X-ray background (Treister & Urry 2006; Gilli et al. 2007) predict that the missing XRB at 30 keV (i.e. the XRB emission that cannot be accounted for by unobscured and moderately obscured AGN) is indeed produced by Compton-thick objects. According to the synthesis model of Gilli et al. (2007), most of the missing XRB is produced by Compton-thick AGN in the redshift interval $z = 0.5$–$1$ and with intrinsic 2–10 keV luminosities in the range $10^{42-44}$ erg s$^{-1}$: these intervals match those of our [Ne v]-selected sample almost perfectly[5].

Our sample is therefore placed in the best position to assess the relevance of Compton-thick AGN to the XRB emission. To this purpose, we used an X-ray stacking analysis to derive the average X/NeV ratio for the 46 X-ray-undetected [Ne v]-selected type 2 AGN (represented by the empty histogram in Fig. 12) and for two subsamples of these X-ray-undetected sources, those with X/NeV < 30 and those with X/NeV > 30. The dividing line of X/NeV = 30 was chosen to have a similar number of objects in both subsamples (22 and 24, respectively). For the 46 X-ray-undetected [Ne v]-selected type 2 AGN, the derived average X/NeV ratio is 9.8 (filled circle in Fig. 12), while for the X/NeV < 30 (X/NeV > 30) subsample the ratio is 3.6 (36). We note that for the first subsample X-ray photometry in the rest-frame 2–10 keV band provides only a 1.6$\sigma$ detection, while for the second subsample we have a 5.8$\sigma$ detection. The results of the stacking analysis were used to tighten the constraints on the Compton-thick AGN fraction among the X-ray-undetected sources as follows: an average of 2.6, 1.1, and 3.9 net counts per source were obtained when stacking the total sample of 46 X-ray-undetected sources, the "faint" subsample of 22 sources with X/NeV < 30, and the "bright" subsample of 24 sources with X/NeV > 30, respectively. We then assumed that the count statistics of the 46 X-ray-undetected sources follows a Poisson distribution with mean 2.6, and verified that this is a good assumption since the integration of the lower and upper half of such a distribution returns average counts of 1.2 and 3.9, which agree excellently with the values measured for the faint and bright subsamples. We then performed $10^4$ Monte Carlo runs, each time randomly extracting 46 count values from the Poisson distribution and converting these counts into X-ray fluxes with the prescriptions given in Sect. 5.1. These random X-ray flux catalogs were associated to the [Ne v] flux catalog of X-ray-undetected sources and the corresponding X/NeV ratios were then computed. By considering the whole set of simulations, on average 29.4 sources (with 2.7 rms) were found to have X/NeV < 15 and are therefore Compton-thick candidates. Based on these simulations, we estimate that the Compton-thick fraction in our sample of 69 type 2 AGN is 43 ± 4%, which is broadly consistent with the expectations from XRB synthesis models (e.g. 50% in Gilli et al. 2007). We stress that the small uncertainties in our estimate of the Compton-thick AGN fraction are just statistical, whereas the systematics related to the selection method and stacking analysis are likely to dominate the error budget. Significant improvements might be obtained by using the data from the recently approved Chandra COSMOS Legacy Survey (2.8 Ms, PI Civano), which will observe the outer portion of the COSMOS field and enlarge the total X-ray coverage to 1.7 deg$^2$ at a depth of 160 ks: the 24 [Ne v]-selected objects that are now outside the Chandra mosaic will then probably be observed, and about half of the current X/NeV upper limits will probably be improved by a factor of 2 (or turn into real measurements) with these new X-ray data. A deeper investigation of the Compton-thick candidates among [Ne v]-selected obscured AGN in COSMOS will be presented in a forthcoming paper (Vignali et al., in prep.), by exploiting both the X-ray techniques (stacking of undetected objects, spectral analysis) and infrared data.

[5] The [Ne v] or [O iii] luminosities were converted into 2–10 keV intrinsic luminosities following the recipes described in Vignali et al. (2010) and Gilli et al. (2010).

## 7. Summary

We have presented a method to select $z \sim 1$ obscured AGN from optical spectroscopic surveys, useful for gathering a more complete census of actively accreting black holes in galaxies. The detection of the high-ionization [Ne v] $\lambda$3426 line was used to pinpoint active nuclei in the 20k-Bright zCOSMOS galaxy sample and we have successfully found systems that escaped other AGN selection techniques.

The [Ne v]-selected type 2 AGN sample consists of 94 sources in the redshift range $0.65 < z < 1.20$, spanning the [O iii] luminosity range $10^{7.5}\,L_\odot < L[\mathrm{O\,III}] < 10^{9.0}\,L_\odot$. The type 2 AGN composite spectrum closely resembles the spectrum of a Seyfert 2 galaxy with strong high-ionization narrow lines. Nevertheless, the line ratios would place it in the transition region of diagnostic diagrams, suggesting some star formation contamination. The mean optical extinction of the narrow-line AGN sample, estimated from the composite H$\beta$/H$\gamma$ flux ratio, is $\langle E(B-V)\rangle = 0.18$. The absorption-line continuum of the composite spectrum, fitted with BC03 population synthesis models, gives information on the average stellar content of the hosts, which roughly corresponds to an Sa/Sb galaxy.

In the same redshift interval, the zCOSMOS survey discovered 60 broad-line AGN, 37 of them with a detected [Ne v] $\lambda$3426 line. Comparing the composite spectra of both the type 1 sample without [Ne v] detection and the [Ne v]-detected type 1 subsample, no significant differences were found. The non-detection of the faint [Ne v] emission line in a fraction of type 1 AGN spectra is therefore probably due to a higher extinction and to the presence of a stronger continuum in these objects, continuum that is shielded in the NL-sample. The two composite spectra do not show peculiar properties either with respect to other known quasar sample.

The main emission lines were also accurately measured in all zCOSMOS spectra of [Ne v]-selected objects. The average [O ii]/[Ne v] flux ratio in the type 2 AGN sample (≈4) is significantly higher than in the type 1 AGN sample (≈2). If interpreted as due to an excess in the [O ii] luminosity, the higher line ratio is suggestive of enhanced star formation in the obscured population, at least with respect to the sample of type 1 AGN.

The stellar masses of galaxy hosts cover the range $5 \times 10^9$–$3 \times 10^{11}\ M_\odot$, and are, on average, higher than those of the galaxy parent sample. The median stellar mass of the type 2 AGN hosts is $8 \times 10^{10}\ M_\odot$, while for the parent galaxy sample it is $3.7 \times 10^{10}\ M_\odot$. The fraction of galaxies hosting

[Ne v]-selected type 2 AGN increases with the stellar mass, reaching a maximum of around 3% at $\approx 2 \times 10^{11}\ M_{\odot}$.

A visual morphological classification was assigned to 71 out of 94 (76%) of the type 2 AGN host galaxies using the ACS images available in COSMOS. Comparing the AGN host morphologies with those of a carefully mass-matched sample of normal galaxies, the two distributions do not look strikingly different, although a possible trend in the relative frequency of the Hubble types seems to emerge: the [Ne v]-selected type 2 AGN do prefer the early-type (Sa-Sb) spiral galaxies, with an expected lack of late-spiral and irregular morphologies. Moreover, a lower fraction of elliptical galaxy hosts, at least with respect to the control sample, is observed. The host galaxy population, which shows later morphologies than brighter type 2 AGN samples (for instance the SDSS sample of Zakamska et al. 2006, who found mainly elliptical hosts), is probably related to the different nuclear luminosity of the samples: our [Ne v]-selected objects cover an [O III] luminosity range at least an order of magnitude fainter than SDDS type 2 quasars.

The selection techniques of type 2 AGN at $z \sim 1$ were also investigated, with a focus on their relative efficiency. First, the [Ne v]-selected sample was compared with the C-COSMOS catalog of X-ray sources: the [Ne v] technique discovered a large fraction of type 2 AGN (46/69, 67%) undetected in the medium-depth, wide-area Chandra survey. Many of these X-ray-faint [Ne v]-emitting galaxies may be heavily obscured active nuclei, especially if we consider that of the 39 zCOSMOS broad-line AGN that fall in the Chandra region, all but two are detected in the X-rays. Conversely, a substantial number of X-ray-luminous galaxies (158) do not show a detectable [Ne v] emission either in single zCOSMOS spectra or in the stacked optical spectrum. Similar results were obtained by comparing [Ne v] and line ratio selection methods: the blue diagnostic diagram, based on [O III]/H$\beta$ versus [O II]/H$\beta$ line ratios, includes 48 [Ne v]-selected type 2 AGN, and again a large fraction of them (29/48, 60%) fall in the star-forming region of the diagram. Likewise, 55 out of 66 (83%) luminous X-ray sources fall in the region of star-forming galaxies. The [Ne v]-selected and X-ray-emitting type 2 AGN share a similar position and class distribution in the [O III]/H$\beta$ versus [O II]/H$\beta$ plane, but these two methods alone cannot provide a fairly complete type 2 AGN selection, since a significant number of emission line galaxies (136) without a visible [Ne v] $\lambda$3426 line in the spectra and undetected in X-rays are classified as active by the diagnostic diagram. Finally, the Mass-Excitation diagnostic diagram seems to be the most comprehensive of the analyzed selection techniques, since more than 50% of the type 2 AGN identified by other methods are classified as AGN according to it. However, MEx-AGN classification may not always hold on an individual galaxy basis, and the degree of contamination is probably the main drawback of the method, as only $\approx$20% of the MEx-AGN candidates are selected by one of the other techniques.

Finally, the 2–10 keV to [Ne v] emission line luminosity ratio was exploited to search for the more heavily obscured AGN. For the 69 [Ne v]-selected type 2 AGN with reliable Chandra measurements, a significant fraction (46 objects, 67%) is undetected in the X-rays and only X/NeV upper limits can be derived. We exploited an X-ray stacking analysis to estimate the average X/NeV ratio for the X-ray-undetected [Ne v]-selected galaxies. A set of Monte Carlo simulations, based on simple assumptions, was performed, finding that the Compton-thick fraction in our sample of type 2 AGN is about 40%, which agrees well with XRB synthesis models (Gilli et al. 2007). Conversely, all 23 X-ray-detected [Ne v]-selected type 2 AGN fall in the region of the Compton-thin objects. We intend to investigate the nature of these Compton-thick AGN candidates in more detail in a forthcoming paper.

*Acknowledgements.* This work was supported by the INAF Grant "PRIN–2010". We also acknowledge financial contribution from the agreement ASI-INAF I/009/10/0. and from the "PRIN–INAF 2011". The authors would like to thank the referee for his/her valuable suggestions and Stéphanie Juneau for helpful discussions and for sharing her results prior to publication.

## References

Aird, J., Coil, A. L., Moustakas, J., et al. 2012, ApJ, 746, 90
Antonucci, R. 1993, ARA&A, 31, 473
Arnaud, K. A. 1996, in Astronomical Data Analysis Software and Systems V, ASP Conf. Ser., 101, 17
Baldwin, J. A. 1977, ApJ, 214, 679
Baldwin, J. A., Phillips, M. M., & Terlevich, R. 1981, PASP, 93, 5
Bolzonella, M., Kovač, K., Pozzetti, L., et al. 2010, A&A, 524, A76
Bongiorno, A., Mignoli, M., Zamorani, G., et al. 2010, A&A, 510, A56
Bongiorno, A., Merloni, A., Brusa, M., et al. 2012, MNRAS, in press
Brandt, W. N., & Hasinger, G. 2005, ARA&A, 43, 827
Broos, P. S., Townsley, L. K., Feigelson, E. D., et al. 2010, ApJ, 714, 1582
Bruzual, G., & Charlot, S. 2003, MNRAS, 344, 1000
Buzzoni, A. 2005, MNRAS, 361, 725
Capak, P., Aussel, H., Ajiki, M., et al. 2007, ApJS, 172, 99
Civano, F., Elvis, M., Brusa, M., et al. 2012, ApJS, 201, 30
Croom, S. M., Smith, R. J., Boyle, B. J., et al. 2004, MNRAS, 349, 1397
Elvis, M., Civano, F., Vignali, C., et al. 2009, ApJS, 184, 158
Ferrarese, L., & Merritt, D. 2000, ApJ, 539, 9
Garilli, B., Fumana, M., Franzetti, P., et al. 2010, PASP, 122, 827
Gavignaud, I., Bongiorno, A., Paltani, S., et al. 2006, A&A, 457, 79
Gebhardt, K., Kormendy, J., Ho, L. C., et al. 2000, ApJ, 543, 5
Gilli, R., Comastri, A., & Hasinger, G. 2007, A&A, 463, 79
Gilli, R., Vignali, C., Mignoli, M., et al. 2010, A&A, 519, A92
Haehnelt, M. G., Madau, P., Kudritzki, R., & Haardt, F. 2001, ApJ, 549, L151
Heckman, T. M. 1980, A&A, 87, 152
Ilbert, O., Tresse, L., Zucca, E., et al. 2005, A&A, 439, 863
Izotov, Y. I., Noeske, K. G., Guseva, N. G., et al. 2004, A&A, 415, L27
Juneau, S., Dickinson, M., Alexander, D. M., & Salim, S. 2011, ApJ, 736, 104
Kauffmann, G., Heckman, T. M., Tremonti, C., et al. 2003, MNRAS, 346, 1055
Koekemoer, A. M., Aussel, H., Calzetti, D., et al. 2007, ApJS, 172, 196
Kormendy, J., & Richstone, D. 1995, ARA&A, 33, 581
Lamareille, F. 2010, A&A, 509, 53
Lamareille, F., Mouhcine, M., Contini, T., et al. 2004, MNRAS, 350, 396
Lamareille, F., Brinchmann, J., Contini, T., et al. 2009, A&A, 495, 53
Lanzuisi, G., Civano, F., Elvis, M., et al. 2013, MNRAS, 431, 978
Le Févre, O., Vettolani, G., Garilli, B., et al. 2005, A&A, 439, 845
Lilly, S. J., Le Févre, O., Renzini, A., et al. 2007, ApJS, 172, 70
Lilly, S. J., Le Brun, V., Maier, C., et al. 2009, ApJS, 184, 218
Magorrian, J., Tremaine, S., Richstone, D., et al. 1998, AJ, 115, 2285
Marconi, A., Risaliti, G., Gilli, R., et al. 2004, MNRAS, 351, 169
McIntosh, D. H., Rix, H.-W., Rieke, M. J., & Foltz, C. B. 1999, ApJ, 517, L73
Mignoli, M., Zamorani, G., Scodeggio, M., et al. 2009, A&A, 493, 39
Moran, E. C., Lehnert, M. D., & Helfand, D. J. 1999, ApJ, 526, 649
Nair, P. B., & Abraham, R. G. 2010, ApJS, 186, 427
Pozzetti, L., Bolzonella, M., Zucca, E., et al. 2010, A&A, 523, A13
Puccetti, S., Vignali, C., Cappelluti, N., et al. 2009, ApJS, 185, 586
Rees, M. J. 1984, ARA&A, 22, 471
Richards, G. T., Strauss, M. A., Fan, X., et al. 2006, AJ, 131, 2766
Rola, C. S., Terlevich, E., & Terlevich, R. J. 1997, MNRAS, 289, 419
Schawinski, K., Urry, C. M., Virani, S., et al. 2010, ApJ, 711, 284
Schmidt, M., Hasinger, G., Gunn, J., et al. 1998, A&A, 329, 495
Scodeggio, M., Franzetti, P., Garilli, B., et al. 2005, PASP, 117, 1284
Scoville, N., Abraham, R. G., Aussel, H., et al. 2007, ApJS, 172, 38
Silverman, J. D., Mainieri, V., Lehmer, B. D., et al. 2008, ApJ, 675, 1025
Silverman, J. D., Lamareille, F., Maier, C., et al. 2009, ApJ, 696, 396
Soltan, A. 1982, MNRAS, 200, 115
Stasiǹska, G., Cid Fernandes, R., Mateus, A., et al. 2006, MNRAS, 371, 972
Treister, E., & Urry, M. C. 2006, ApJ, 652, L79
Tremaine, S., Gebhardt, K., Bender, R., et al. 2002, ApJ, 574, 740
Vanden Berk, D. E., Richards, G. T., Bauer, A., et al. 2001, AJ, 122, 549
Vignali, C., Alexander, D. M., Gilli, R., & Pozzi, F. 2010, MNRAS, 404, 48
Zakamska, N. L., Strauss, M. A., Krolik, J. H., et al. 2006, AJ, 132, 1496
Zamorani, G., Marano, B., Mignoli, M., et al. 1992, MNRAS, 200, 115
Zucca, E., Bardelli, S., Bolzonella, M., et al. 2009, A&A, 508, 1217